Metabolomic and [superscript 13]C-metabolic flux analysis of a xylose-consuming Saccharomyces cerevisiae strain expressing xylose isomerase

Citation: Wasylenko, Thomas M., and Gregory Stephanopoulos. "Metabolomic and 13 C-Metabolic Flux Analysis of a Xylose-Consuming Saccharomyces Cerevisiae Strain Expressing Xylose Isomerase: Xylose Metabolic Flux Analysis." Biotechnology and Bioengineering 112.3 (2015): 470–483.

As Published: http://dx.doi.org/10.1002/bit.25447

Publisher: Wiley Blackwell

Persistent URL: http://hdl.handle.net/1721.1/109764

Version: Author's final manuscript: final author's manuscript post peer review, without publisher's formatting or copy editing

HHS Public Access

Author manuscript

Biotechnol Bioeng. Author manuscript; available in PMC 2016 March 21.

Published in final edited form as:

Biotechnol Bioeng. 2015 March ; 112(3): 470–483. doi:10.1002/bit.25447.

Metabolomic and ^{13}C-Metabolic Flux Analysis of a Xylose-Consuming *Saccharomyces cerevisiae* Strain Expressing Xylose Isomerase

Thomas M. Wasylenko and **Gregory Stephanopoulos**

Department of Chemical Engineering, Massachusetts Institute of Technology, Cambridge, MA 02139, USA

Abstract

Over the past two decades significant progress has been made in the engineering of xylose-consuming *Saccharomyces cerevisiae* strains for production of lignocellulosic biofuels. However, the ethanol productivities achieved on xylose are still significantly lower than those observed on glucose for reasons that are not well understood. We have undertaken an analysis of central carbon metabolite pool sizes and metabolic fluxes on glucose and on xylose under aerobic and anaerobic conditions in a strain capable of rapid xylose assimilation via xylose isomerase in order to investigate factors that may limit the rate of xylose fermentation. We find that during xylose utilization the flux through the non-oxidative PPP is high but the flux through the oxidative PPP is low, highlighting an advantage of the strain employed in this study. Furthermore, xylose fails to elicit the full carbon catabolite repression response that is characteristic of glucose fermentation in *S. cerevisiae*. We present indirect evidence that the incomplete activation of the fermentation program on xylose results in a bottleneck in lower glycolysis, leading to inefficient re-oxidation of NADH produced in glycolysis.

Keywords

^{13}C-Metabolic Flux Analysis; Carbon Catabolite Repression; Cellulosic Ethanol; Metabolomics; *Saccharomyces cerevisiae*; Xylose

Introduction

In recent years, increasing energy demand and concerns about climate change and the sustainability of heavy reliance on fossil fuels have motivated the development of technologies for production of liquid fuels from plant biomass. Ethanol, which serves as a fuel additive, can be readily produced by fermentation of hexose sugars derived from cornstarch and sucrose. However, production of feed stocks such as corn and sugarcane requires large amounts of arable land and may compete with the food supply.

Correspondence: Prof. Gregory Stephanopoulos, Dept. of Chemical Engineering, Massachusetts Institute of Technology, Room 56-469C, 77 Massachusetts Ave, Cambridge, MA 02139, Phone: (617) 253-4583, Fax: (617) 253-3122, gregstep@mit.edu.

Conflict of Interest

The authors declare that they have no conflict of interest.

Lignocellulosic feed stocks represent an attractive alternative, but technologies for production of liquid fuels from lignocellulosic material are relatively immature. The Baker's yeast *Saccharomyces cerevisiae* is a promising biocatalyst for production of liquid fuels from lignocellulosic biomass because its high rates of ethanol production under anaerobic conditions and high ethanol tolerance allow ethanol to be produced at high yield, productivity, and final titer. *S. cerevisiae* also exhibits relatively high tolerance to inhibitors such as furan derivatives, weak acids, and phenolics present in lignocellulosic hydrolysates (Almeida et al., 2007; Lau et al., 2010), and the insusceptibility of yeast to bacteriophage and its ability to grow at low pH minimize the risk of contamination, allowing the avoidance of costs associated with reactor sterilization in industrial processes. However *S. cerevisiae* cannot natively metabolize the pentose sugars xylose and arabinose, which make up more than one-third of the carbohydrate biomass in some agricultural residues such as corn stover, wheat straw, and bagasse, with xylose being by far the more abundant of the two (van Maris et al., 2006). For production of biofuels from lignocellulosic feed stocks to be cost-effective, it will be necessary to effect the conversion of all sugars present in hydrolysates to liquid fuels (Stephanopoulos, 2007; Carroll and Somerville, 2009).

The ability to consume xylose can be conferred on *S. cerevisiae* strains by introduction of a heterologous pathway for conversion of xylose to its isomer xylulose. While many bacteria use a xylose isomerase (XI) enzyme to catalyze this conversion directly without the use of pyridine nucleotide cofactors, xylose-consuming eukaryotes generally effect the isomerization through a two-step redox pathway in which xylose reductase (XR) first catalyzes the reduction of xylose to xylitol, which is then oxidized via xylitol dehydrogenase (XDH) to form xylulose. Initial attempts to express heterologous *xylA* (encoding XI) genes in *S. cerevisiae* were unsuccessful; in several cases putative *xylA* transcripts were detected in Northern blots but putative XI protein products were insoluble and inactive (Sarthy et al., 1987; Amore et al., 1989; Gárdonyi and Hahn-Hägerdal, 2003). Consequently, the majority of xylose-consuming strains have been constructed using the XR-XDH pathway. However, while XR uses NADPH as its preferred cofactor substrate, XDH is strictly NAD^+-dependent. This mismatch in cofactor specificities results in a "cofactor imbalance" whereby $NADP^+$ and NADH accumulate (and NADPH and NAD^+ are depleted). The accumulation of NADH is especially problematic under industrially relevant anaerobic conditions. Without oxygen as a terminal electron acceptor, NADH cannot be efficiently re-oxidized to NAD^+, severely inhibiting xylose metabolism (Bruinenberg et al., 1983; Bruinenberg et al., 1984). In early xylose-consuming *S. cerevisiae* strains the low availability of NAD^+ for the XDH reaction also resulted in secretion of large amounts of the by-product xylitol (Kötter and Ciriacy, 1993; Tantirungkij et al., 1993), compromising ethanol yield.

A major breakthrough occurred with the discovery that the anaerobic fungus *Piromyces* sp. strain E2 metabolizes xylose using the XI pathway (Harhangi et al., 2003). The XI from this organism was functionally expressed in *S. cerevisiae* (Kuyper et al., 2003), and both evolutionary and rational metabolic engineering were used to construct efficient xylose-consuming strains capable of anaerobic growth on xylose (Kuyper et al., 2004; Kuyper et al., 2005a; Kuyper et al., 2005b). Our lab has recently used a similar approach along with a multi-stage evolutionary strategy to engineer the *S. cerevisiae* strain H131-A3-AL^{CS}, the

fastest xylose-consuming strain reported to date (Zhou et al., 2012). However, the rates of growth and ethanol production on xylose are still significantly lower than those on glucose for reasons that are not completely understood.

Many hypotheses for bottlenecks in xylose metabolism have been presented. These include xylose transport, which may be especially limiting at low extracellular xylose concentrations (Gárdonyi et al., 2003; Runquist et al., 2009a; Runquist et al., 2010; Young et al., 2012); conversion of xylose to xylulose (Lönn et al., 2003; Jeppsson et al., 2003; Karhumaa et al., 2005; Kim et al., 2012); phosphorylation of xylulose (Toivari et al., 2001; Jin et al., 2003); and conversion of xylulose-5-phosphate (X5P) to the glycolytic intermediates fructose-6-phosphate (F6P) and glyceraldehyde-3-phosophate (GAP) via the reactions of the non-oxidative Pentose Phosphate Pathway (PPP) (Walfridsson et al., 1995; Kuyper et al., 2005a). Once xylose is metabolized to F6P and GAP xylose metabolism is in principle identical to glucose metabolism. However while glucose induces a strong carbon catabolite repression (CCR) response in *S. cerevisiae* (Gancedo, 2008), there is evidence that xylose is not recognized as a fermentable carbon source and fails to fully activate the CCR program (Jin et al., 2004; Salusjärvi et al., 2008). Consequently, bottlenecks downstream of GAP could result from altered gene expression during xylose utilization.

In this study, we sought to characterize the metabolism of strain H131-A3-AL^{CS} by quantifying central carbon metabolite pool sizes and using ^{13}C-Metabolic Flux Analysis (MFA) to estimate the fluxes through central metabolism in order to identify rate-limiting steps in xylose utilization. Although previous metabolomic and MFA studies have been conducted on xylose-consuming *S. cerevisiae* strains, many of these studies investigated strains that utilized the XR-XDH pathway to effect xylose isomerization (Wahlbom et al., 2001; Pitkänen et al., 2003; Sonderegger et al., 2004; Grotkjaer et al., 2005; Klimacek et al., 2010; Feng and Zhao, 2013a; Feng and Zhao, 2013b; Matsushika et al., 2013). Consequently, in these strains the redox cofactor imbalance is expected to exert a large influence on metabolism. Moreover, many of the strains employed exhibited low xylose consumption rates and growth rates, and in several cases analysis of metabolite pool sizes revealed signs of carbon starvation (Klimacek et al., 2010; Bergdahl et al., 2012; Matsushika et al., 2013). In this study, we investigated a strain capable of rapid xylose utilization via the xylose isomerase pathway in order to observe the differences between glucose and xylose metabolism under aerobic and anaerobic conditions with high rates of xylose consumption and in the absence of the redox cofactor imbalance associated with action of the XR-XDH pathway. We present indirect evidence that in this strain there is an apparent bottleneck in xylose metabolism downstream of GAP, in the lower glycolysis pathway.

Materials and Methods

Strain and Culture Conditions

All experiments were performed with a previously engineered xylose-consuming *S. cerevisiae* strain similar to H131-A3-AL^{CS} (Zhou et al., 2012). The strain was cultivated at 30 °C in minimal medium containing 6.7 g/l Yeast Nitrogen Base (YNB) without amino acids (Difco) as a source of salts, vitamins, and trace elements and 20 g/l of either glucose (YNBG) or xylose (YNBX) as the sole carbon source. Media were supplemented with 0.42

g/l Tween 80 and 0.01 g/l ergosterol to facilitate growth under anaerobic conditions (Andreasen and Stier, 1953; Andreasen and Stier, 1954).

The yeast strain was cultivated in both YNBG and YNBX medium under both aerobic and anaerobic conditions, resulting in a total of four culture conditions: Glucose Aerobic (GA), Glucose Anaerobic (GN), Xylose Aerobic (XA), and Xylose Anaerobic (XN). For each culture condition, 5 ml starter cultures were inoculated from 15% glycerol −80 °C freezer stocks. 50 ml main cultures grown in 250 ml bottles (VWR, 89000-236) were inoculated with 50 μl (0.1% by volume) of the starter culture with the same carbon source and aeration condition. All cultures were shaken at 250 rpm to facilitate mixing.

Aerobic starter cultures were grown in aerobic culture tubes (BD Falcon, #352059). The 250 ml aerobic main culture bottle caps were left loose, allowing exchange between the culture headspace and the (aerobic) ambient atmosphere. Anaerobic starter cultures were grown in airtight Hungate tubes (ChemGlass, #CLS-4208-01). Anaerobic starter culture media were sparged with Ultra High Purity (UHP) Nitrogen (Airgas) for 3 min and left in an anaerobic chamber (Coy Labs) under an atmosphere of nitrogen and hydrogen for approximately 12 h prior to inoculation. Anaerobic main cultures were grown with 250 ml bottle caps completely tightened, preventing aeration from the ambient atmosphere. Anaerobic main culture media were sparged with UHP Nitrogen for 15 min and left in the anaerobic chamber for 12 h prior to inoculation. Inoculation and all sampling were conducted inside the anaerobic chamber.

For ^{13}C-MFA, the YNBG and YNBX carbon sources were 20 g/l 1,2-$^{13}C_2$-glucose and 20 g/l 1,2-$^{13}C_2$-xylose (Cambridge Isotope Laboratories), respectively. The ^{13}C-MFA cultures were otherwise identical.

Analytical Methods

Cell density was monitored by measuring the absorbance (“optical density”) of yeast cultures at 600 nm (OD_{600}) using an Ultrospec 2100 *pro* UV/Visible Spectrophotometer (Amersham Biosciences). Cell density was calculated using pre-determined correlations between Dry Cell Weight (DCW) and OD_{600}. Glucose, xylose, ethanol, glycerol, and acetate concentrations were determined by High-Performance Liquid Chromatography (HPLC). Culture samples were filtered through 0.20 μm Nylon syringe filters (Microliter Analytical #F13-2020-1GF) and supernatants were analyzed on an Agilent 1200 series HPLC system equipped with a refractive index detector. Analytes were separated on an Aminex HPX-87H column (Bio-Rad) with 5 mM sulfuric acid mobile phase at a flow rate of 0.6 ml/min and a temperature of 55 °C.

Estimation of Extracellular Fluxes

Specific growth rates, specific sugar consumption rates, and specific ethanol, glycerol, and acetate production rates were estimated from OD_{600} and HPLC data from five biological replicate cultures for each culture condition. For each biological replicate culture *j* the specific growth rate μ_j was determined by fitting the OD_{600} data to a function of the form:

$$\mathrm{OD}(t)=\mathrm{OD}_0\exp(\mu_j t)$$

where $OD(t)$ is the measured value of OD_{600} at time t and OD_0 is the fitted value of OD_{600} at time zero. Parameter estimation was achieved using the Matlab function lsqnonlin.

To determine specific metabolite consumption and production rates for biological replicate culture j, the concentration of each metabolite k was plotted against OD_{600} and the slope of the best-fit line m_{jk} was computed. For each culture condition the average specific growth rate μ and the average slope m_k were computed by averaging the μ_j and m_{jk}, respectively. Uncertainties were assumed to be equal to the standard deviations of the μ_j and m_{jk}. The specific consumption or production rate of metabolite k is then equal to:

$$q_k=\frac{m_k\mu}{k_{\mathrm{DCW}}}$$

where k_{DCW} is the biomass concentration that is equivalent to one OD_{600} unit. The relative error in q_k was assumed to be equal to the sum of the relative errors in μ, m_k and k_{DCW}.

Preparation of Uniformly ^{13}C-Labeled Cell Extract for Internal Standard

Cells were grown in medium containing 10 g/l U-$^{13}C_6$-glucose as the sole carbon source and 6.7 g/l YNB without amino acids. 5 ml aerobic starter cultures were inoculated from freezer stocks (as above). 40 ml shake flask cultures were inoculated from starter cultures and harvested at OD_{600} ~ 1. Uniformly ^{13}C-labeled metabolite extracts were prepared using a protocol similar to the one described for preparation of samples for pool size measurements and ^{13}C-MFA (see below). Extracts were stored at −80 °C and subsequently dried under airflow using a Pierce Reacti-Therm III Heating/Stirring Module and resuspended in 100 μl Millipore water. A total of 48 extracts (four extracts from each of 12 shake flasks) were pooled and the pooled cell extract was aliquoted. Aliquots were stored at −80 °C for future use as internal standard.

Metabolite Extractions for Pool Size Measurements and ^{13}C-Metabolic Flux Analysis

Cultures were harvested in mid-exponential phase (OD_{600} ~ 0.5–0.6). 7.5 ml culture was quenched in 37.5 ml pure methanol (Canelas et al., 2008) held at low temperature (<−70 °C) in a cold ethanol bath. Samples were centrifuged for 5 min at 3270*g* and −10 °C. Centrifuge adapters for holding sample tubes were pre-cooled in a −80 °C freezer to keep the sample temperature as low as possible during centrifugation. The supernatants were discarded and cell pellets were washed by resuspension in 40 ml cold (<−70 °C) methanol. Samples were centrifuged a second time and supernatants discarded. 50 μl ^{13}C-labeled cell extract was added to cell pellets for pool size measurement samples (which are labeled to natural abundance) only for use as internal standard (Wu et al., 2005). Internal standard solution was not added to ^{13}C-labeled samples for MFA.

A hot ethanol extraction (Gonzalez et al., 1997; Canelas et al., 2009) was used for extraction of intracellular metabolites. 5 ml hot (80 °C) 75% (v/v) ethanol solution was added to each

cell pellet and samples were vortexed for 30 s, incubated in an 80 °C water bath for 3 min, and vortexed a second time for 30 s. Samples were briefly cooled in the cold (<−70 °C) ethanol bath and centrifuged to remove cell debris. 3.5 ml supernatant was set aside for LC-MS/MS analysis and the remaining supernatant (~ 1.5 ml) was used for GC/MS analysis. Metabolite extracts were stored at −80 °C and subsequently dried under airflow using a Pierce Reacti-Therm III Heating/Stirring Module prior to GC/MS and LC-MS/MS analysis.

Gas Chromatography/Mass Spectrometry (GC/MS)

All metabolites without phosphate groups (organic acids and amino acids) were analyzed by GC/MS. Dried metabolite extracts were resuspended in 20 µl 2% methoxyamine-hydrogen chloride in pyridine (Methoxamine (MOX) Reagent, Thermo Scientific #TS-45950) and incubated at 37 °C for 1.5 h. Following the methoximation reaction, 30 µl *N*-*tert*-Butyldimethylsilyl-*N*-methyltrifluoroacetamide with 1% *tert*-Butyldimethylchlorosilane (Sigma-Aldrich, #375934) was added to each sample and samples were incubated at 55 °C for 1 h. The resulting *tert*-butyldimethylsilyl derivates were analyzed by GC/MS using an Agilent 6890N Network GC System coupled to an Agilent 5975B Inert XL MSD. 1 µl sample was injected in splitless mode with an inlet temperature of 270 °C. Metabolite separation was achieved using an Agilent J&W DB-35ms column (#122-3832, 30.0 m × 250 µm × 0.25 µm) with helium carrier gas at a flow rate of 1 ml/min. The GC column oven temperature was initially held at 100 °C for 1 min, ramped to 105 °C at 2.5 °C/min, held at 105 °C for 2 min, ramped to 250 °C at 3.5 °C/min and then to 320 °C at 20 °C/min, for a total run time of approximately 50 min. The MS was operated in electron ionization mode with an electron energy of 69.9 eV and source and quadrupole temperatures of 230 °C and 150 °C, respectively. Mass spectra were measured by scanning the range 100–650 m/z.

Liquid Chromatography/Tandem Mass Spectrometry (LC-MS/MS)

All phosphorylated metabolites (sugar phosphates from glycolysis and the PPP, acetyl-CoA, and all cofactors depicted in Fig. 3) were analyzed by LC-MS/MS. Dried metabolite extracts were resuspended in 80 µl Millipore water and analyzed using an ion pair chromatography method adapted from (Luo et al., 2007). Metabolite separation was achieved with an Agilent 1100 Series HPLC system using a Waters XBridge C18 Column (2.1 mm × 150 mm, 130 Å, 3.5 µm; #186003023). Metabolite isotopomers were quantified with an API 2000 MS/MS (AB Sciex) operating in multiple reaction monitoring (MRM) mode. The injection volume was 20 µl. The majority of samples were run at an increased flow rate of 300 µl/min with a fast gradient similar to that employed by (Young et al., 2011) in order to increase sample throughput.

Quantification of Metabolite Pool Sizes

Pool size measurements were conducted in biological triplicate with technical duplicates for each of the three biological replicates. Accurate quantification was achieved using uniformly ^{13}C-labeled metabolite extract as internal standard. Internal standard was added to calibration standards as well as samples so that calibration curves could be constructed in terms of the ratio of the M+0 (from sample) and M+N (from internal standard) isotopomer peak areas (where N is the number of carbons in the metabolite backbone) (Wu et al., 2005).

Metabolic Flux Estimation

A model metabolic network was constructed for estimation of intracellular metabolic fluxes. The model network consisted of the reactions of Glycolysis, the PPP, the Tricarboxylic Acid (TCA) Cycle, One-Carbon Metabolism, pathways for xylose assimilation and ethanol, glycerol, and acetate production, and biosynthetic pathways for synthesis of biomass constituents. The reactions of the non-oxidative PPP were modeled using half-reactions as in (Kleijn et al., 2005). The composition of *S. cerevisiae* biomass was taken from (Förster et al., 2003). For anaerobic cultures it was assumed unsaturated fatty acids and sterols were taken up from the medium rather than synthesized from the sugar carbon source (Andreasen and Stier, 1953; Andreasen and Stier, 1954) and the biomass equation was adjusted accordingly. The modeling of compartmentalization was similar to that in (Maaheimo et al., 2001); both cytosolic and mitochondrial pools of pyruvate, acetyl-CoA, and oxaloacetate were included in the model, the anaplerotic pyruvate carboxylase reaction was assumed to occur in the cytosol, and the malic enzyme reaction was assumed to occur in the mitochondria. As in (Maaheimo et al., 2001), pyruvate transport was assumed to be unidirectional, from cytosol to mitochondria. However, oxaloacetate transport was assumed to occur in both directions in order to represent the possible impact of the malate-aspartate (or malate-oxaloacetate) shuttle on metabolite labeling patterns. Both cytosolic and mitochondrial reactions were included for alanine aminotransferase. The reactions of the metabolic model and relevant atom transitions are listed in Supplementary Table S1.

For flux estimation, an in-house elementary metabolite unit (EMU)-based software was used to simulate the extracellular flux and mass spectrometry metabolite labeling data predicted to result from a given flux distribution (Antoniewicz et al., 2007a). The shift in mass isotopomer distribution (MID) mole fractions expected to result from natural abundance of heavy isotopes was accounted for by including naturally occurring heavy isotopes in simulations (Wittmann and Heinzle, 1999; van Winden et al., 2002). Reversible reactions were modeled in terms of net and exchange fluxes rather than forward and backward fluxes (Wiechert and de Graaf, 1997). For each culture condition, the best estimate for the true metabolic flux distribution was computed by minimizing the lack-of-fit between experimentally measured and simulated datasets. Only metabolite MIDs which could be measured with high accuracy were included in the MFA. In the GC/MS and LC-MS/MS analysis, control samples labeled to natural abundance were analyzed side-by-side with ^{13}C-labeled samples. The MIDs of the metabolites in the natural abundance samples can be predicted from theory, and MIDs which could not be measured to sufficient accuracy in these samples were excluded from the flux estimation models. In some cases, a metabolite pool size could be quantified by measuring the M+0 isotopomer in samples labeled to natural abundance, but the metabolite MID could not be measured to sufficient accuracy for MFA because of interference by co-eluting molecules that overlapped with higher isotopomers or because the MS signal was not sufficiently high to accurately quantify less abundant isotopomers.

Each flux estimation was performed 500 times with random initial guesses and the flux distribution with the lowest weighted sum-of-squared residuals was assumed to be the global optimum. A chi-square test for goodness-of-fit was used to evaluate whether each flux

model adequately described the data, and nonlinear 68% and 95% confidence intervals were computed for each estimated flux by computing the sensitivity of the weighted sum-of-squared residuals to variations in the flux value (Antoniewicz et al., 2006). For the chi-square test and confidence interval computation, an error of 0.325 mol % was assumed for the mole fractions in the MID data, which is reasonable given the expected measurement (Antoniewicz et al., 2007b) and modeling (Wasylenko and Stephanopoulos, 2013) errors. The assumed errors for extracellular fluxes were discussed above.

Results and Discussion

Estimation of Extracellular Fluxes

The metabolism of the xylose-consuming strain was studied under Glucose Aerobic (GA), Glucose Anaerobic (GN), Xylose Aerobic (XA), and Xylose Anaerobic (XN) culture conditions in order to investigate the effects of carbon source and aeration on metabolism. The specific growth rates, specific metabolite consumption and production rates, and their uncertainties were computed from OD_{600} and HPLC data from five biological replicate experiments for each culture condition. The values used for the flux estimation algorithm are listed in Table I. It can be seen that glucose carbon source and aerobic conditions allowed faster growth than xylose and anaerobic conditions, respectively. However the growth rates in the GA, XA, and GN conditions were relatively similar while the growth rate in the XN condition was significantly lower than the rest. Specific sugar consumption and ethanol production rates were higher with glucose as carbon source (relative to xylose) and under anaerobic conditions (relative to aerobic conditions). Glycerol production was significantly increased under anaerobic conditions on both carbon sources. This was expected as glycerol serves as an electron sink, and its production allows for regeneration of NAD^+ when oxygen is not available as a terminal electron acceptor. Acetate production was low under all conditions tested.

Metabolite Pool Size Measurements and Metabolic Flux Estimation

Central carbon metabolite pool sizes were measured under each of the four culture conditions. The results for metabolites of Glycolysis and the PPP, metabolites of the TCA Cycle, and select nucleotide cofactors are shown in Figs. 1, 2, and 3, respectively. The high ratio of glucose-6-phosphate (G6P) to F6P during growth on glucose (4.3 aerobic, 6.4 anaerobic) and the high adenylate energy charge under all conditions (>0.90) suggest metabolism was satisfactorily quenched during sample preparation (Ewald et al., 2009).

The intracellular metabolic flux distribution for each culture condition was estimated by fitting OD_{600} and HPLC data and metabolite labeling data obtained from GC-MS and LC-MS/MS to a metabolic model. The best-fit metabolic flux distributions are shown in Fig. 4. The Weighted Sums of Squared Residuals (WSSRs) from the parameter estimations are shown in Fig. 5. It can be seen that for each of the four culture conditions the WSSR falls in the range that would be expected from the assumption that the WSSR is drawn from a chi-square distribution, suggesting the model adequately describes the data. WSSRs for model variants are also shown and are discussed below. The measured and simulated ^{13}C-labeling data for the best-fit flux models can be compared in Supplementary Table S2. Non-linear

68% and 95% flux confidence intervals were computed and are shown for select fluxes in Fig. 6. The complete set of best-fit fluxes and confidence intervals is presented in Supplementary Table S3. The pool size and flux estimation results are discussed below, with the results organized by metabolic pathway.

Pentose Phosphate Pathway

It can be seen that when xylose is the sole carbon source the flux through the non-oxidative PPP is more than one order of magnitude higher than when glucose is the sole carbon source (Fig. 4). This is a direct result of the metabolic network topology. All carbon assimilated from xylose enters central metabolism at X5P and consequently must pass through the reactions of the non-oxidative PPP. In contrast, during growth on glucose the majority of carbon flux is channeled through glycolysis with only a fraction being diverted through the PPP to allow production of NADPH for biosynthesis and formation of ribose-5-phosphate (R5P) and erythrose-4-phosophate (E4P) carbon backbones which serve as precursors for amino acids and nucleotides. It has been shown that PPP flux in yeasts metabolizing glucose correlates with biomass yield, likely because high biomass yields increase demand for NADPH produced in the oxidative PPP (Blank et al., 2005). Under fermentative conditions in which the majority of carbon is converted to ethanol the PPP flux on glucose is expected to be low (Gombert et al., 2001; Fiaux et al., 2003). The increased flux through the non-oxidative PPP on xylose results in a significant increase in the pool sizes of the metabolites of this pathway (Fig. 1), consistent with previous observations in *S. cerevisiae* during pentose utilization (Kötter and Ciriacy, 1993; Wisselink et al., 2010).

In contrast, the flux through the oxidative PPP is low under all conditions (Figs. 4, 6). Carbon from xylose need not pass through this phase of the PPP to be assimilated into central metabolism. Previous work with strains employing the XR-XDH pathway for xylose assimilation has suggested that the flux through the oxidative PPP is high during xylose utilization, likely due to the redox cofactor imbalance which increases demand for NADPH (Pitkänen et al., 2003; Sonderegger et al., 2004; Grotkjaer et al., 2005; Runquist et al., 2009b; Feng and Zhao, 2013a). The high flux through this pathway decreases the ethanol yield that can be achieved with these strains because one mole of carbon is lost as CO_2 for every two moles of NADPH produced (Pitkänen et al., 2003; Grotkjaer et al., 2005). Because XI is used to effect the conversion of xylose to xylulose in the strain investigated here, the redox balance in the cell is not perturbed by xylose assimilation and only minimal flux through the oxidative PPP is required to satisfy NADPH demand; consequently higher ethanol yields can be obtained. Low oxidative PPP flux has also been found in an arabinose-consuming strain of *S. cerevisiae* utilizing an isomerase pathway for arabinose assimilation (Wisselink et al., 2010).

Glycolysis

Carbon derived from xylose via the non-oxidative PPP enters the glycolytic pathway at F6P and GAP, with the PPP stoichiometry dictating that roughly two moles of F6P are produced for every mole of GAP. (The ratio deviates slightly from 2:1 due to withdrawal of R5P and E4P for biosynthesis). Because carbon enters the pathway below the G6P node, the flux through phosphoglucose isomerase (PGI) is reversed during xylose utilization, with a net

flux from F6P to G6P to allow synthesis of carbohydrates and small flux through the oxidative PPP (Figs. 4, 6). This reversal of flux results in a depletion of the G6P pool during growth on xylose, which is especially remarkable under anaerobic conditions (Fig. 1). The majority of F6P derived from xylose is directed to GAP through the upper glycolytic pathway, although this flux is somewhat attenuated on xylose because some carbon from the non-oxidative PPP is converted to GAP directly. Once GAP is formed, the pathways for glucose and xylose utilization are identical.

Tricarboxylic Acid Cycle

The fluxes through the TCA Cycle are observed to be low in all conditions, as the majority of carbon from pyruvate is converted to ethanol rather than being transported to the mitochondria and oxidized to form CO_2. Under anaerobic conditions the TCA Cycle is essentially inactive, and the reactions of the pathway serve only to provide carbon building blocks for biosynthesis. The flux through α-ketoglutarate dehydrogenase (KGD) is estimated to be zero and the flux through succinate dehydrogenase (SDH) is minimal (Figs. 4, 6). (The small flux through SDH is a result of formation of succinate as a by-product of cysteine biosynthesis.) The lack of flux through the TCA Cycle is expected under anaerobic conditions since oxygen is not available as a terminal electron acceptor for re-oxidation of mitochondrial NADH, and it can be seen that the pool sizes of metabolites in this pathway depend more on aeration than carbon source (Fig. 2). In the GA condition there is a small flux through KGD, but inspection of the flux confidence intervals reveals that this flux is not significantly different from zero (Fig. 6). This minimal flux through the TCA Cycle under the GA condition is likely a result of glucose-repression of this pathway (Polakis and Bartley, 1965), and is consistent with previous work in *S. cerevisiae* under fermentative conditions (Gombert et al., 2001). Only in the XA case do the labeling data suggest a significant (albeit still small) flux through KGD (Fig. 6).

Incomplete Activation of Fermentation Program

The small but significant flux through the TCA Cycle in the XA condition suggests an incomplete induction of the CCR response, which has previously been observed during xylose assimilation (Jin et al., 2004; Salusjärvi et al., 2008). Other glucose-repressed metabolic pathways include gluconeogenesis, the glyoxylate shunt, and oxidative phosphorylation. Previous transcriptomic studies of H131-A3-AL^{CS} (Zhou et al., 2012) and other xylose-consuming strains (Wahlbom et al., 2003; Jin et al., 2004; Salusjärvi et al., 2008; Runquist et al., 2009b; Scalcinati et al., 2012) have revealed upregulation of genes associated with these pathways during growth on xylose. Inclusion of the glyoxylate shunt in the metabolic network did not significantly affect the results of flux estimation. The WSSRs for the models with and without this pathway were virtually identical in all cases (Fig. 5), and when the glyoxylate shunt was included the estimated flux through the pathway was negligible (data not shown). Thus, the labeling data do not provide any evidence for the activity of this pathway.

The labeling data do suggest that the gluconeogenic enzyme fructose-1,6-bisphosphatase (FBPase1) is active during growth on xylose. FBPase1 essentially catalyzes the reverse of the reaction catalyzed by phosphofructokinase-1 (Pfk1), which is coupled to ATP hydrolysis

and consequently practically irreversible. The activation of FBPase1 is modeled by making the Pfk1 reaction for conversion of F6P to fructose-1,6-bisphosphate (FBP) reversible. Although the exchange flux (equivalent to the backward flux for a reversible reaction) for the Pfk1 reaction could not be resolved, Fig. 5 shows that when FBPase1 was excluded from the model (i.e. when the Pfk1 reaction was specified as irreversible) a dramatic increase in the WSSRs for the xylose flux estimation models was observed. This implies that the model without FBPase1 does not describe the xylose labeling datasets as well as the model that includes FBPase1. The large increases in the WSSRs resulted from an inability to fit the F6P labeling data without the FBPase1 reaction in the model (data not shown). However, it can be seen that when FBPase1 was omitted from the glucose flux estimation models the effect was relatively small, and the WSSRs still fell in the range expected from the chi-square distribution. Thus the data provide evidence for activity of FBPase1 on xylose but not on glucose.

In *S. cerevisiae*, FBPase1 flux is repressed in the presence of glucose through several redundant mechanisms, as futile cycling between Pfk1 and FBPase1 is detrimental to the cell (Navas and Gancedo, 1996). The transcription of the associated gene FBP1 is repressed and the degradation of FBP1 mRNA accelerated in the presence of even low concentrations of glucose. This effect can be triggered by the extracellular glucose sensor Snf3 or the Ras-cAMP pathway (Yin et al., 2000). It has also been proposed that accumulation of G6P (which was depleted on xylose; see above) prevents localization of Snf1 to the nucleus, contributing to the repression of gluconeogenic genes (Vincent et al., 2001), and previous work suggests that accumulation of G6P and F6P is both necessary and sufficient for complete repression of FBPase1 activity (Gancedo and Gancedo, 1979). The FBPase1 protein is also degraded in the presence of glucose (Belinchón and Gancedo, 2007), and FBPase1 activity is inhibited by accumulation of fructose-2,6-bisphosphate (F-2,6-BP), which is an allosteric inhibitor and also stimulates the phosphorylation and inactivation of the enzyme by protein kinase A (PKA) (Gancedo et al., 1983). The accumulation of F-2,6-BP in the presence of glucose is itself a result of PKA-dependent phosphorylation and activation of phosphofructokinase-2 (Pfk2) (Vaseghi et al., 2001; Dihazi et al., 2003). PKA can be activated by the extracellular glucose sensor Gpr1 or the Ras-cAMP pathway (Rolland et al., 2000; Gancedo, 2008). Activation of the Ras-cAMP pathway has been shown to be dependent on glucose phosphorylation (Rolland et al., 2000) and may be incomplete on xylose due to the depletion of G6P. Thus the increased FBPase1 flux on xylose likely results from some combination of absence of stimulation of the extracellular glucose sensors Gpr1, Rgt2, and Snf3, incomplete activation of the Ras-cAMP pathway, and depletion of G6P which possibly results in nuclear localization of Snf1.

Although expression of FBPase1 on xylose would be expected to result in futile cycling between Pfk1 and FBPase1 and unnecessary ATP expenditure, the high energy charges in XA and XN conditions (Fig. 3) suggest that this has little impact on xylose metabolism. The gluconeogenic enzyme PEP carboxykinase (PEPCK) was also shown to be upregulated in H131-A3-AL^{CS} (Zhou et al., 2012), but was not included in the metabolic model because in the glucose flux models the flux through this enzyme could not be resolved; the flux through the cycle formed by pyruvate kinase, pyruvate carboxylase, and PEPCK could be arbitrarily

large without exerting a significant influence on metabolite labeling patterns (data not shown). When PEPCK was included in either xylose flux model the estimated flux was zero, indicating that if the enzyme is active it may not carry significant flux.

The data also indicate the exchange flux for transport of oxaloacetate (OAA) across the mitochondrial membrane is increased on xylose. While the transport of OAA from mitochondria to cytosol is not significant during growth on glucose, it is on xylose (Figs. 4 and 6), particularly under anaerobic conditions. Fig. 5 shows that the WSSRs were increased in the xylose flux estimation models when OAA transport from cytosol to mitochondria was modeled as an irreversible reaction. The effect was again more pronounced under anaerobic conditions, where the WSSR of the irreversible OAA transport model fell outside the range expected from the chi-square distribution, suggesting reversible OAA transport is necessary to satisfactorily describe the XN labeling data.

The biological significance of the increased OAA transport exchange flux on xylose is not obvious. OAA transport into the mitochondria is driven by the proton gradient and is generally unidirectional (Palmieri et al., 1999; Maaheimo et al., 2001). The increased exchange flux on xylose could represent export of four carbon units from the TCA Cycle to the cytosol due to incomplete repression of gluconeogenic pathways. The labeling data also could be explained by synthesis of aspartate by mitochondrial aspartate aminotransferase (in the metabolic model aspartate was assumed to be synthesized exclusively in the cytosol, as in (Maaheimo et al., 2001)). However, an attractive explanation is that the high OAA transport exchange flux is a result of shuttling of NADH equivalents across the mitochondrial membrane. Several redox shuttles that effectively transport NADH equivalents across the mitochondrial membrane exist in *S. cerevisiae*. These include the malate-aspartate shuttle, the malate-oxaloacetate shuttle, and the ethanol-acetaldehyde shuttle. In eukaryotes, the malate-aspartate shuttle generally transports NADH equivalents generated in the cytosol (e.g. by glycolysis) into the mitochondria for oxidative phosphorylation, and may be able to operate against a concentration gradient. The latter two shuttles can in principle transport reducing equivalents in either direction but likely not against a concentration gradient (Bakker et al., 2001).

Operation of the malate-aspartate (or malate-oxaloacetate) shuttle would have an effect on metabolite labeling distributions similar to that of reversible OAA transport. Although the malate-aspartate shuttle exists in *S. cerevisiae* (Cavero et al., 2003), it is associated with respiratory metabolism and is not expected to carry significant flux during glucose fermentation, when NADH is re-oxidized primarily by ethanol formation rather than oxidative phosphorylation. Previous work has shown the cytosolic malate dehydrogenase Mdh2, a key component of the pathway and also of the malate-oxaloacetate shuttle, is inactive during growth on glucose (Minard and McAlister-Henn, 1992; Minard and McAlister-Henn, 1994). On xylose, activation of Mdh2 due to incomplete induction of CCR could result in increased redox shuttling activity. This possibility is discussed below.

Lower Glycolysis as a Potential Bottleneck in Xylose Metabolism

The *S. cerevisiae* strain employed in this study exhibited a specific growth rate in the XN condition that was significantly lower than those observed in the other three conditions,

indicating the presence of bottlenecks in anaerobic xylose metabolism. It can be seen that there were significant increases in both the GAP pool size (Fig. 1) and the exchange flux for the triosephosphate isomerase (TPI) reaction (Figs. 4, 6) in the XN condition. Taken together, these data suggest the presence of a bottleneck downstream of GAP, which causes GAP to accumulate and increases the rate of the back reaction to DHAP. The 2-phosphoglycerate/3-phosphateglycerate (2/3PG) and phosphoenolpyruvate (PEP) pools were depleted in the XN condition, suggesting the bottleneck occurs in lower glycolysis.

A bottleneck in lower glycolysis could result from incomplete activation of the fermentation program on xylose. Although the signaling mechanisms for activation of CCR are complex and incompletely understood, intracellular metabolite concentrations likely play a prominent role (Belinchón and Gancedo, 2003; Gancedo, 2008). In particular, accumulation of G6P (as well as other glycolytic metabolites) has been shown to be required for complete activation of enzymes associated with lower glycolysis and ethanol formation (Boles et al., 1993; Boles and Zimmermann, 1993; Müller et al., 1995; Boles et al., 1996). It was noted above that the G6P pool was depleted in the XN condition, so it is plausible that the activities of lower glycolytic enzymes are reduced during xylose utilization. Previous transcriptomic studies have revealed decreased expression of several lower glycolytic genes on xylose relative to on glucose (Wahlbom et al., 2003; Jin et al., 2004), and a transcriptomic analysis of H131-A3-AL^{CS} resulted in similar findings, although the changes in expression were not significant (i.e. less than two-fold) (Zhou et al., 2012).

Under fermentative conditions, cytosolic NADH produced in the GAP dehydrogenase (GAPDH) reaction is re-oxidized largely through ethanol formation. Consequently, a bottleneck in lower glycolysis or ethanologenesis might lead to inefficient regeneration of cytosolic NAD^+. Under aerobic conditions a bottleneck in cytosolic NADH re-oxidation could be alleviated by shuttling NADH into the mitochondria, where it could be re-oxidized in the electron transport chain with oxygen as the terminal electron acceptor. However under anaerobic conditions inefficient ethanol formation would likely result in accumulation of NADH and low NAD^+ availability. Fig. 3 shows that the NADH pool size was indeed increased (and the NAD^+/NADH ratio decreased) in the XN condition relative to all other conditions. The low availability of NAD^+ would then limit the rate of the GAPDH reaction, consistent with the observed accumulation of GAP, increased TPI exchange flux, and depletion of 2/3PG and PEP pools.

Interestingly, on xylose Matsushika, *et al*. observed even more dramatic accumulation of metabolites upstream of GAP and depletion of metabolites downstream of GAP than those reported here (Matsushika et al., 2013). The study employed a strain that utilized the XR-XDH pathway to effect xylose isomerization. Consequently, in this strain the NAD^+ availability would be expected to be very low due to the redox cofactor imbalance associated with that pathway. The authors concluded that low glycolytic flux limited the rate of xylose utilization. Although they did not measure the pool sizes of NAD^+ or NADH, our data suggest that in their study also the glycolytic flux may have been limited by the availability of NAD^+ for the GAPDH reaction.

Inefficient re-oxidation and accumulation of NADH could also explain the apparent increased flux of NADH equivalents across the mitochondrial membrane discussed above. Under aerobic conditions the best-fit OAA transport exchange flux was slightly increased on xylose relative to glucose (Fig. 4), and the flux confidence intervals reveal that this flux is significantly different from zero on xylose but not on glucose (Fig. 6). Under XA conditions, NADH equivalents could be shuttled into the mitochondria via the malate-aspartate (or malate-oxaloacetate) shuttle and oxidized in the electron transport chain. The increased NADH shuttling activity would likely result from activation of Mdh2 due to incomplete CCR, inefficient oxidation of NADH in the cytosol due to low activities of enzymes in lower glycolysis and ethanologenesis, or a combination of the two.

Surprisingly the increase in OAA transport exchange flux is more pronounced in the XN condition, where oxygen is not available as a terminal electron acceptor and NADH equivalents shuttled into the mitochondria cannot be efficiently re-oxidized in the electron transport chain. However, we note that the flux of NADH equivalents into the mitochondria is relatively low. In the XN condition the best-fit OAA transport exchange flux is only 0.50 mmol/g/h while the flux through GAPDH is 17.89 mmol/g/h. Thus, only a few percent of the NADH equivalents generated in glycolysis would be shuttled into the mitochondria. The NADH shuttling flux may be higher under anaerobic conditions because the glycolytic flux (and the rate of NADH production) is higher, increasing the burden on the lower glycolytic and ethanologenic pathways for NAD^+ regeneration. It is unclear how the NADH shuttled into the mitochondria would be re-oxidized, but several redox shuttling systems exist in *S. cerevisiae*, as noted above. One interesting possibility is that the mitochondrial alcohol dehydrogenase Adh3 may catalyze the conversion of acetaldehyde to ethanol in the mitochondria. It has previously been proposed that under anaerobic conditions Adh3 oxidizes NADH generated in the mitochondria by amino acid biosynthesis (Nissen et al., 1997).

Taken together then, the data suggest that in the strain employed here slow metabolism of GAP to pyruvate and ultimately to ethanol and inefficient re-oxidation of NADH produced in glycolysis may limit xylose consumption under anaerobic conditions, where oxygen is unavailable to serve as an electron acceptor for regeneration of NAD^+. The presence of the bottleneck in lower glycolysis hypothesized here would most likely arise due to the extensive engineering of strain H131-A3-AL^{CS}. Upon introduction of the xylose assimilation pathway, bottlenecks are far more likely to occur in xylose transport or conversion to the glycolytic metabolites F6P and GAP. However, overexpression of *xylA*, *XYL3*, and the genes of the non-oxidative PPP along with multi-stage evolutionary engineering which resulted in a multi-copy integration of *xylA* into the chromosome (Zhou et al., 2012) appear to have removed all bottlenecks in the assimilation of xylose to central carbon metabolism. Consequently, the changes in gene expression that result from incomplete CCR on xylose may have become the dominant factor in limiting the rate of xylose metabolism.

Because CCR is a complex phenomenon, it is not obvious how one would engineer a yeast strain with a fully active fermentation program during metabolism of xylose as sole carbon source. If glycolytic metabolite pool sizes do play a role in regulation, it would be difficult

to recapitulate the metabolite profile from glucose fermentation on xylose due to differences in reaction network topology. It may be possible to realize faster xylose consumption by engineering the promoters of genes associated with lower glycolysis and ethanol formation to achieve higher activities during xylose utilization. For biofuels applications, another strategy may be to engineer strains that consume the glucose and xylose in biomass hydrolysates simultaneously. Such an approach would allow metabolism of xylose with glucose present to support flux though upper glycolysis, allowing for larger pools of metabolites in that pathway, and activate the fermentation program. Although glucose represses xylose uptake, an interesting strategy for co-fermentation of cellobiose and xylose has recently been presented (Ha et al., 2011). Such approaches hold much promise for production of lignocellulosic biofuels.

Supplementary Material

Refer to Web version on PubMed Central for supplementary material.

Acknowledgments

We acknowledge financial support from Shell Oil. TMW was supported by the MIT/NIGMS Biotechnology Training Program.

References

Almeida JR, Modig T, Petersson A, Hähn-Hägerdal B, Lidén G, Gorwa-Grauslund MF. Increased tolerance and conversion of inhibitors in lignocellulosic hydrolysates bySaccharomyces cerevisiae. J Chem Technol Biotechnol. 2007; 82:340–349.

Amore R, Wilhelm M, Hollenberg CP. The fermentation of xylose--an analysis of the expression of Bacillus and Actinoplanes xylose isomerase genes in yeast. Appl Microbiol Biotechnol. 1989; 30:351–357.

Andreasen AA, Stier TJ. Anaerobic nutrition of Saccharomyces cerevisiae. II. Unsaturated fatty acid requirement for growth in a defined medium. J Cell Physiol. 1954; 43:271–281. [PubMed: 13192151]

Andreasen AA, Stier TJB. Anaerobic nutrition of Saccharomyces cerevisiae. I. Ergosterol requirement for growth in a defined medium. J Cell Physiol. 1953; 41:23–36. [PubMed: 13034889]

Antoniewicz MR, Kelleher JK, Stephanopoulos G. Determination of confidence intervals of metabolic fluxes estimated from stable isotope measurements. Metab Eng. 2006; 8:324–337. [PubMed: 16631402]

Antoniewicz MR, Kelleher JK, Stephanopoulos G. Elementary metabolite units (EMU): a novel framework for modeling isotopic distributions. Metab Eng. 2007a; 9:68–86. [PubMed: 17088092]

Antoniewicz MR, Kelleher JK, Stephanopoulos G. Accurate assessment of amino acid mass isotopomer distributions for metabolic flux analysis. Anal Chem. 2007b; 79:7554–7559. [PubMed: 17822305]

Bakker BM, Overkamp KM, van Maris AJnull, Kötter P, Luttik MA, van Dijken JP, null Pronk JT. Stoichiometry and compartmentation of NADH metabolism in Saccharomyces cerevisiae. FEMS Microbiol Rev. 2001; 25:15–37. [PubMed: 11152939]

Belinchón MM, Gancedo JM. Xylose and some non-sugar carbon sources cause catabolite repression in Saccharomyces cerevisiae. Arch Microbiol. 2003; 180:293–297. [PubMed: 12955310]

Belinchón MM, Gancedo JM. Glucose controls multiple processes in Saccharomyces cerevisiae through diverse combinations of signaling pathways. FEMS Yeast Res. 2007; 7:808–818. [PubMed: 17428308]

Bergdahl B, Heer D, Sauer U, Hahn-Hägerdal B, van Niel EW. Dynamic metabolomics differentiates between carbon and energy starvation in recombinant Saccharomyces cerevisiae fermenting xylose. Biotechnol Biofuels. 2012; 5:34. [PubMed: 22587303]

Blank LM, Lehmbeck F, Sauer U. Metabolic-flux and network analysis in fourteen hemiascomycetous yeasts. FEMS Yeast Res. 2005; 5:545–558. [PubMed: 15780654]

Boles E, Heinisch J, Zimmermann FK. Different signals control the activation of glycolysis in the yeast Saccharomyces cerevisiae. Yeast Chichester Engl. 1993; 9:761–770.

Boles E, Müller S, Zimmermann FK. A multi-layered sensory system controls yeast glycolytic gene expression. Mol Microbiol. 1996; 19:641–642. [PubMed: 8830254]

Boles E, Zimmermann FK. Induction of pyruvate decarboxylase in glycolysis mutants of Saccharomyces cerevisiae correlates with the concentrations of three-carbon glycolytic metabolites. Arch Microbiol. 1993; 160:324–328. [PubMed: 8239883]

Bruinenberg PM, Bot PHM, Dijken JP, Scheffers WA. The role of redox balances in the anaerobic fermentation of xylose by yeasts. Eur J Appl Microbiol Biotechnol. 1983; 18:287–292.

Bruinenberg P, Bot PM, Dijken J, Scheffers WA. NADH-linked aldose reductase: the key to anaerobic alcoholic fermentation of xylose by yeasts. Appl Microbiol Biotechnol. 1984; 19:256–260.

Canelas AB, ten Pierick A, Ras C, Seifar RM, van Dam JC, van Gulik WM, Heijnen JJ. Quantitative evaluation of intracellular metabolite extraction techniques for yeast metabolomics. Anal Chem. 2009; 81:7379–7389. [PubMed: 19653633]

Canelas AB, Ras C, Pierick A, Dam JC, Heijnen JJ, Gulik WM. Leakage-free rapid quenching technique for yeast metabolomics. Metabolomics. 2008; 4:226–239.

Carroll A, Somerville C. Cellulosic biofuels. Annu Rev Plant Biol. 2009; 60:165–182. [PubMed: 19014348]

Cavero S, Vozza A, del Arco A, Palmieri L, Villa A, Blanco E, Runswick MJ, Walker JE, Cerdán S, Palmieri F, Satrústegui J. Identification and metabolic role of the mitochondrial aspartate-glutamate transporter in Saccharomyces cerevisiae. Mol Microbiol. 2003; 50:1257–1269. [PubMed: 14622413]

Dihazi H, Kessler R, Eschrich K. Glucose-induced stimulation of the Ras-cAMP pathway in yeast leads to multiple phosphorylations and activation of 6-phosphofructo-2-kinase. Biochemistry (Mosc). 2003; 42:6275–6282.

Ewald JC, Heux S, Zamboni N. High-throughput quantitative metabolomics: workflow for cultivation, quenching, and analysis of yeast in a multiwell format. Anal Chem. 2009; 81:3623–3629. [PubMed: 19320491]

Feng X, Zhao H. Investigating xylose metabolism in recombinant Saccharomyces cerevisiae via 13C metabolic flux analysis. Microb Cell Factories. 2013a; 12:114.

Feng X, Zhao H. Investigating glucose and xylose metabolism in *Saccharomyces cerevisiae* and *Scheffersomyces stipitis* via ^{13}C metabolic flux analysis. AIChE J. 2013b; 59:3195–3202.

Fiaux J, Cakar ZP, Sonderegger M, Wüthrich K, Szyperski T, Sauer U. Metabolic-flux profiling of the yeasts Saccharomyces cerevisiae and Pichia stipitis. Eukaryot Cell. 2003; 2:170–180. [PubMed: 12582134]

Förster J, Famili I, Fu P, Palsson BØ, Nielsen J. Genome-scale reconstruction of the Saccharomyces cerevisiae metabolic network. Genome Res. 2003; 13:244–253. [PubMed: 12566402]

Gancedo JM, Gancedo C. Inactivation of gluconeogenic enzymes in glycolytic mutants of Saccharomyces cerevisiae. Eur J Biochem FEBS. 1979; 101:455–460.

Gancedo JM, Mazón MJ, Gancedo C. Fructose 2,6-bisphosphate activates the cAMP-dependent phosphorylation of yeast fructose-1,6-bisphosphatase in vitro. J Biol Chem. 1983; 258:5998–5999. [PubMed: 6304022]

Gancedo JM. The early steps of glucose signalling in yeast. FEMS Microbiol Rev. 2008; 32:673–704. [PubMed: 18559076]

Gárdonyi M, Hahn-Hägerdal B. The Streptomyces rubiginosus xylose isomerase is misfolded when expressed in Saccharomyces cerevisiae. Enzyme Microb Technol. 2003; 32:252–259.

Gárdonyi M, Jeppsson M, Lidén G, Gorwa-Grauslund MF, Hahn-Hägerdal B. Control of xylose consumption by xylose transport in recombinant Saccharomyces cerevisiae. Biotechnol Bioeng. 2003; 82:818–824. [PubMed: 12701148]

Gombert AK, Moreira dos Santos M, Christensen B, Nielsen J. Network identification and flux quantification in the central metabolism of Saccharomyces cerevisiae under different conditions of glucose repression. J Bacteriol. 2001; 183:1441–1451. [PubMed: 11157958]

Gonzalez B, François J, Renaud M. A rapid and reliable method for metabolite extraction in yeast using boiling buffered ethanol. Yeast Chichester Engl. 1997; 13:1347–1355.

Grotkjaer T, Christakopoulos P, Nielsen J, Olsson L. Comparative metabolic network analysis of two xylose fermenting recombinant Saccharomyces cerevisiae strains. Metab Eng. 2005; 7:437–444. [PubMed: 16140032]

Ha S-J, Galazka JM, Kim SR, Choi J-H, Yang X, Seo J-H, Glass NL, Cate JHD, Jin Y-S. Engineered Saccharomyces cerevisiae capable of simultaneous cellobiose and xylose fermentation. Proc Natl Acad Sci USA. 2011; 108:504–509. [PubMed: 21187422]

Harhangi HR, Akhmanova AS, Emmens R, van der Drift C, de Laat WTAM, van Dijken JP, Jetten MSM, Pronk JT, Op den Camp HJM. Xylose metabolism in the anaerobic fungus Piromyces sp. strain E2 follows the bacterial pathway. Arch Microbiol. 2003; 180:134–141. [PubMed: 12811467]

Jeppsson M, Träff K, Johansson B, Hahn-Hägerdal B, Gorwa-Grauslund MF. Effect of enhanced xylose reductase activity on xylose consumption and product distribution in xylose-fermenting recombinant Saccharomyces cerevisiae. FEMS Yeast Res. 2003; 3:167–175. [PubMed: 12702449]

Jin Y-S, Laplaza JM, Jeffries TW. Saccharomyces cerevisiae engineered for xylose metabolism exhibits a respiratory response. Appl Environ Microbiol. 2004; 70:6816–6825. [PubMed: 15528549]

Jin Y-S, Ni H, Laplaza JM, Jeffries TW. Optimal growth and ethanol production from xylose by recombinant Saccharomyces cerevisiae require moderate D-xylulokinase activity. Appl Environ Microbiol. 2003; 69:495–503. [PubMed: 12514033]

Karhumaa K, Hahn-Hägerdal B, Gorwa-Grauslund M-F. Investigation of limiting metabolic steps in the utilization of xylose by recombinant Saccharomyces cerevisiae using metabolic engineering. Yeast Chichester Engl. 2005; 22:359–368.

Kim SR, Ha S-J, Kong II, Jin Y-S. High expression of XYL2 coding for xylitol dehydrogenase is necessary for efficient xylose fermentation by engineered Saccharomyces cerevisiae. Metab Eng. 2012; 14:336–343. [PubMed: 22521925]

Kleijn RJ, van Winden WA, van Gulik WM, Heijnen JJ. Revisiting the 13C–label distribution of the non-oxidative branch of the pentose phosphate pathway based upon kinetic and genetic evidence. FEBS J. 2005; 272:4970–4982. [PubMed: 16176270]

Klimacek M, Krahulec S, Sauer U, Nidetzky B. Limitations in xylose-fermenting Saccharomyces cerevisiae, made evident through comprehensive metabolite profiling and thermodynamic analysis. Appl Environ Microbiol. 2010; 76:7566–7574. [PubMed: 20889786]

Kötter P, Ciriacy M. Xylose fermentation by Saccharomyces cerevisiae. Appl Microbiol Biotechnol. 1993; 38:776–783.

Kuyper M, Harhangi HR, Stave AK, Winkler AA, Jetten MSM, de Laat WTAM, den Ridder JJJ, Op den Camp HJM, van Dijken JP, Pronk JT. High-level functional expression of a fungal xylose isomerase: the key to efficient ethanolic fermentation of xylose by Saccharomyces cerevisiae? FEMS Yeast Res. 2003; 4:69–78. [PubMed: 14554198]

Kuyper M, Hartog MMP, Toirkens MJ, Almering MJH, Winkler AA, van Dijken JP, Pronk JT. Metabolic engineering of a xylose-isomerase-expressing Saccharomyces cerevisiae strain for rapid anaerobic xylose fermentation. FEMS Yeast Res. 2005a; 5:399–409. [PubMed: 15691745]

Kuyper M, Toirkens MJ, Diderich JA, Winkler AA, van Dijken JP, Pronk JT. Evolutionary engineering of mixed-sugar utilization by a xylose-fermenting Saccharomyces cerevisiae strain. FEMS Yeast Res. 2005b; 5:925–934. [PubMed: 15949975]

Kuyper M, Winkler AA, van Dijken JP, Pronk JT. Minimal metabolic engineering of Saccharomyces cerevisiae for efficient anaerobic xylose fermentation: a proof of principle. FEMS Yeast Res. 2004; 4:655–664. [PubMed: 15040955]

Lau MW, Gunawan C, Balan V, Dale BE. Comparing the fermentation performance of Escherichia coli KO11, Saccharomyces cerevisiae 424A(LNH-ST) and Zymomonas mobilis AX101 for cellulosic ethanol production. Biotechnol Biofuels. 2010; 3:11. [PubMed: 20507563]

Lönn A, Träff-Bjerre K, Cordero Otero R, van Zyl W, Hahn-Hägerdal B. Xylose isomerase activity influences xylose fermentation with recombinant Saccharomyces cerevisiae strains expressing mutated xylA from Thermus thermophilus. Enzyme Microb Technol. 2003; 32:567–573.

Luo B, Groenke K, Takors R, Wandrey C, Oldiges M. Simultaneous determination of multiple intracellular metabolites in glycolysis, pentose phosphate pathway and tricarboxylic acid cycle by liquid chromatography-mass spectrometry. J Chromatogr A. 2007; 1147:153–164. [PubMed: 17376459]

Maaheimo H, Fiaux J, Cakar ZP, Bailey JE, Sauer U, Szyperski T. Central carbon metabolism of Saccharomyces cerevisiae explored by biosynthetic fractional (13)C labeling of common amino acids. Eur J Biochem FEBS. 2001; 268:2464–2479.

Van Maris AJA, Abbott DA, Bellissimi E, van den Brink J, Kuyper M, Luttik MAH, Wisselink HW, Scheffers WA, van Dijken JP, Pronk JT. Alcoholic fermentation of carbon sources in biomass hydrolysates by Saccharomyces cerevisiae: current status. Antonie Van Leeuwenhoek. 2006; 90:391–418. [PubMed: 17033882]

Matsushika A, Nagashima A, Goshima T, Hoshino T. Fermentation of xylose causes inefficient metabolic state due to carbon/energy starvation and reduced glycolytic flux in recombinant industrial Saccharomyces cerevisiae. PloS One. 2013; 8:e69005. [PubMed: 23874849]

Minard KI, McAlister-Henn L. Glucose-induced degradation of the MDH2 isozyme of malate dehydrogenase in yeast. J Biol Chem. 1992; 267:17458–17464. [PubMed: 1324938]

Minard KI, McAlister-Henn L. Glucose-induced phosphorylation of the MDH2 isozyme of malate dehydrogenase in Saccharomyces cerevisiae. Arch Biochem Biophys. 1994; 315:302–309. [PubMed: 7986072]

Müller S, Boles E, May M, Zimmermann FK. Different internal metabolites trigger the induction of glycolytic gene expression in Saccharomyces cerevisiae. J Bacteriol. 1995; 177:4517–4519. [PubMed: 7635834]

Navas MA, Gancedo JM. The regulatory characteristics of yeast fructose-1,6-bisphosphatase confer only a small selective advantage. J Bacteriol. 1996; 178:1809–1812. [PubMed: 8606152]

Nissen TL, Schulze U, Nielsen J, Villadsen J. Flux distributions in anaerobic, glucose-limited continuous cultures of Saccharomyces cerevisiae. Microbiol Read Engl. 1997; 143:203–218.

Palmieri L, Vozza A, Agrimi G, De Marco V, Runswick MJ, Palmieri F, Walker JE. Identification of the yeast mitochondrial transporter for oxaloacetate and sulfate. J Biol Chem. 1999; 274:22184–22190. [PubMed: 10428783]

Pitkänen J-P, Aristidou A, Salusjärvi L, Ruohonen L, Penttilä M. Metabolic flux analysis of xylose metabolism in recombinant Saccharomyces cerevisiae using continuous culture. Metab Eng. 2003; 5:16–31. [PubMed: 12749841]

Polakis ES, Bartley W. Changes in the enzyme activities of Saccharomyces cerevisiae during aerobic growth on different carbon sources. Biochem J. 1965; 97:284–297. [PubMed: 16749116]

Rolland F, De Winde JH, Lemaire K, Boles E, Thevelein JM, Winderickx J. Glucose-induced cAMP signalling in yeast requires both a G-protein coupled receptor system for extracellular glucose detection and a separable hexose kinase-dependent sensing process. Mol Microbiol. 2000; 38:348–358. [PubMed: 11069660]

Runquist D, Fonseca C, Rådström P, Spencer-Martins I, Hahn-Hägerdal B. Expression of the Gxf1 transporter from Candida intermedia improves fermentation performance in recombinant xylose-utilizing Saccharomyces cerevisiae. Appl Microbiol Biotechnol. 2009a; 82:123–130. [PubMed: 19002682]

Runquist D, Hahn-Hägerdal B, Bettiga M. Increased expression of the oxidative pentose phosphate pathway and gluconeogenesis in anaerobically growing xylose-utilizing Saccharomyces cerevisiae. Microb Cell Factories. 2009b; 8:49.

Runquist D, Hahn-Hägerdal B, Rådström P. Comparison of heterologous xylose transporters in recombinant Saccharomyces cerevisiae. Biotechnol Biofuels. 2010; 3:5. [PubMed: 20236521]

Salusjärvi L, Kankainen M, Soliymani R, Pitkänen J-P, Penttilä M, Ruohonen L. Regulation of xylose metabolism in recombinant Saccharomyces cerevisiae. Microb Cell Factories. 2008; 7:18.

Sarthy AV, McConaughy BL, Lobo Z, Sundstrom JA, Furlong CE, Hall BD. Expression of the Escherichia coli xylose isomerase gene in Saccharomyces cerevisiae. Appl Environ Microbiol. 1987; 53:1996–2000. [PubMed: 2823706]

Scalcinati G, Otero JM, Van Vleet JRH, Jeffries TW, Olsson L, Nielsen J. Evolutionary engineering of Saccharomyces cerevisiae for efficient aerobic xylose consumption. FEMS Yeast Res. 2012; 12:582–597. [PubMed: 22487265]

Sonderegger M, Jeppsson M, Hahn-Hägerdal B, Sauer U. Molecular basis for anaerobic growth of Saccharomyces cerevisiae on xylose, investigated by global gene expression and metabolic flux analysis. Appl Environ Microbiol. 2004; 70:2307–2317. [PubMed: 15066826]

Stephanopoulos G. Challenges in engineering microbes for biofuels production. Science. 2007; 315:801–804. [PubMed: 17289987]

Tantirungkij M, Nakashima N, Seki T, Yoshida T. Construction of xylose-assimilating Saccharomyces cerevisiae. J Ferment Bioeng. 1993; 75:83–88.

Toivari MH, Aristidou A, Ruohonen L, Penttilä M. Conversion of xylose to ethanol by recombinant Saccharomyces cerevisiae: importance of xylulokinase (XKS1) and oxygen availability. Metab Eng. 2001; 3:236–249. [PubMed: 11461146]

Vaseghi S, Macherhammer F, Zibek S, Reuss M. Signal transduction dynamics of the protein kinase-A/phosphofructokinase-2 system in Saccharomyces cerevisiae. Metab Eng. 2001; 3:163–172. [PubMed: 11289792]

Vincent O, Townley R, Kuchin S, Carlson M. Subcellular localization of the Snf1 kinase is regulated by specific beta subunits and a novel glucose signaling mechanism. Genes Dev. 2001; 15:1104–1114. [PubMed: 11331606]

Wahlbom CF, Eliasson A, Hahn-Hägerdal B. Intracellular fluxes in a recombinant xylose-utilizing Saccharomyces cerevisiae cultivated anaerobically at different dilution rates and feed concentrations. Biotechnol Bioeng. 2001; 72:289–296. [PubMed: 11135198]

Wahlbom CF, Cordero Otero RR, van Zyl WH, Hahn-Hägerdal B, Jönsson LJ. Molecular analysis of a Saccharomyces cerevisiae mutant with improved ability to utilize xylose shows enhanced expression of proteins involved in transport, initial xylose metabolism, and the pentose phosphate pathway. Appl Environ Microbiol. 2003; 69:740–746. [PubMed: 12570990]

Walfridsson M, Hallborn J, Penttilä M, Keränen S, Hahn-Hägerdal B. Xylose-metabolizing Saccharomyces cerevisiae strains overexpressing the TKL1 and TAL1 genes encoding the pentose phosphate pathway enzymes transketolase and transaldolase. Appl Environ Microbiol. 1995; 61:4184–4190. [PubMed: 8534086]

Wasylenko TM, Stephanopoulos G. Kinetic isotope effects significantly influence intracellular metabolite (13) C labeling patterns and flux determination. Biotechnol J. 2013; 8:1080–1089. [PubMed: 23828762]

Wiechert W, de Graaf AA. Bidirectional reaction steps in metabolic networks: I. Modeling and simulation of carbon isotope labeling experiments. Biotechnol Bioeng. 1997; 55:101–117. [PubMed: 18636449]

Van Winden WA, Wittmann C, Heinzle E, Heijnen JJ. Correcting mass isotopomer distributions for naturally occurring isotopes. Biotechnol Bioeng. 2002; 80:477–479. [PubMed: 12325156]

Wisselink HW, Cipollina C, Oud B, Crimi B, Heijnen JJ, Pronk JT, van Maris AJA. Metabolome, transcriptome and metabolic flux analysis of arabinose fermentation by engineered Saccharomyces cerevisiae. Metab Eng. 2010; 12:537–551. [PubMed: 20816840]

Wittmann, Heinzle. Mass spectrometry for metabolic flux analysis. Biotechnol Bioeng. 1999; 62:739–750. [PubMed: 10099575]

Wu L, Mashego MR, van Dam JC, Proell AM, Vinke JL, Ras C, van Winden WA, van Gulik WM, Heijnen JJ. Quantitative analysis of the microbial metabolome by isotope dilution mass spectrometry using uniformly 13C–labeled cell extracts as internal standards. Anal Biochem. 2005; 336:164–171. [PubMed: 15620880]

Yin Z, Hatton L, Brown AJ. Differential post-transcriptional regulation of yeast mRNAs in response to high and low glucose concentrations. Mol Microbiol. 2000; 35:553–565. [PubMed: 10672178]

Young EM, Comer AD, Huang H, Alper HS. A molecular transporter engineering approach to improving xylose catabolism in Saccharomyces cerevisiae. Metab Eng. 2012; 14:401–411. [PubMed: 22445945]

Young JD, Shastri AA, Stephanopoulos G, Morgan JA. Mapping photoautotrophic metabolism with isotopically nonstationary (13)C flux analysis. Metab Eng. 2011; 13:656–665. [PubMed: 21907300]

Zhou H, Cheng J-S, Wang BL, Fink GR, Stephanopoulos G. Xylose isomerase overexpression along with engineering of the pentose phosphate pathway and evolutionary engineering enable rapid xylose utilization and ethanol production by Saccharomyces cerevisiae. Metab Eng. 2012; 14:611–622. [PubMed: 22921355]

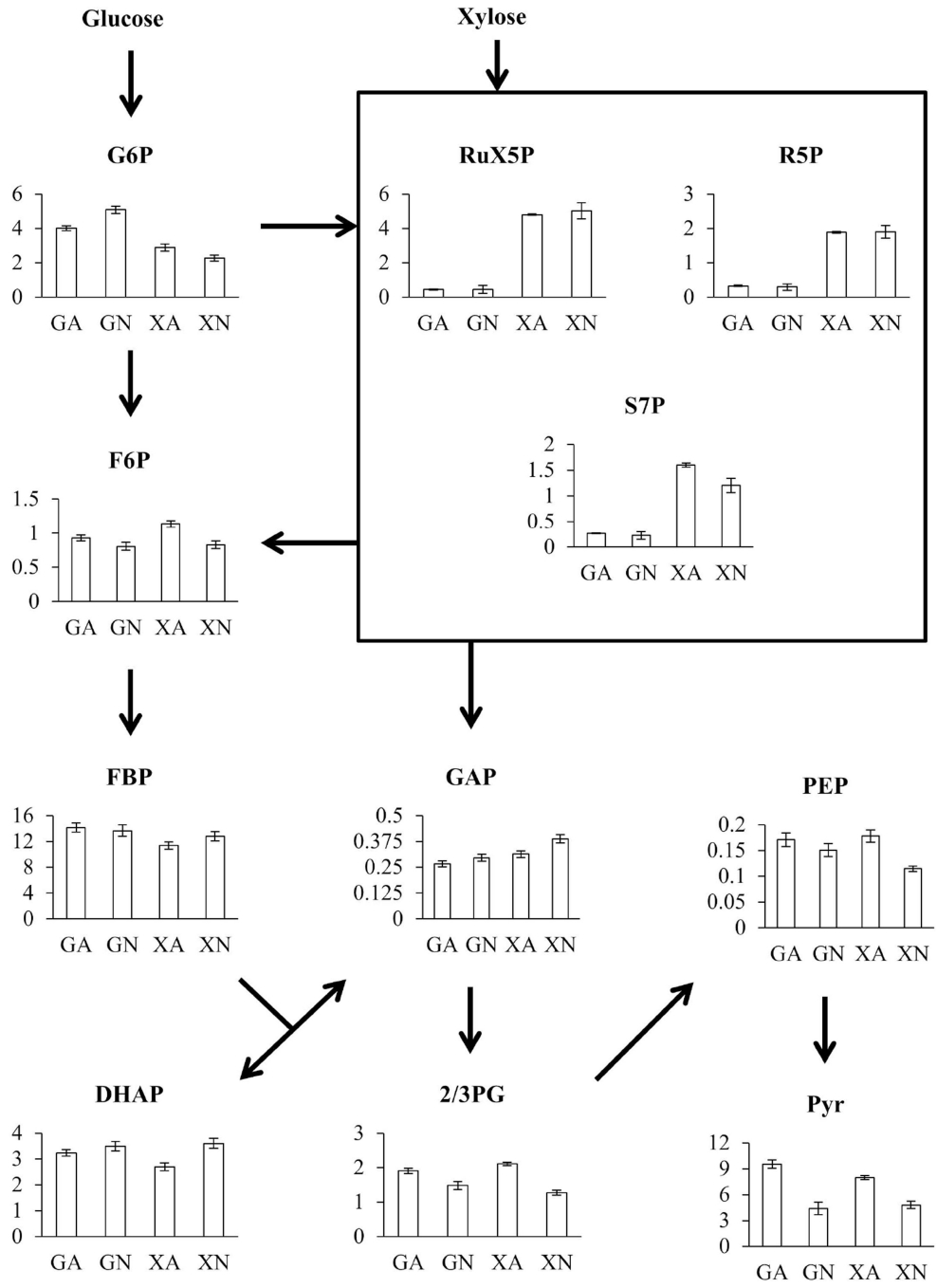

Fig. 1.

Metabolite pool sizes for metabolites in Glycolysis and the PPP. All pool sizes are in units of μmol/g DCW. Error bars represent uncertainties from standard deviations of three biological replicates as well as uncertainties in OD_{600}-DCW correlations. GA = Glucose Aerobic, GN = Glucose Anaerobic, XA = Xylose Aerobic, XN = Xylose Anaerobic

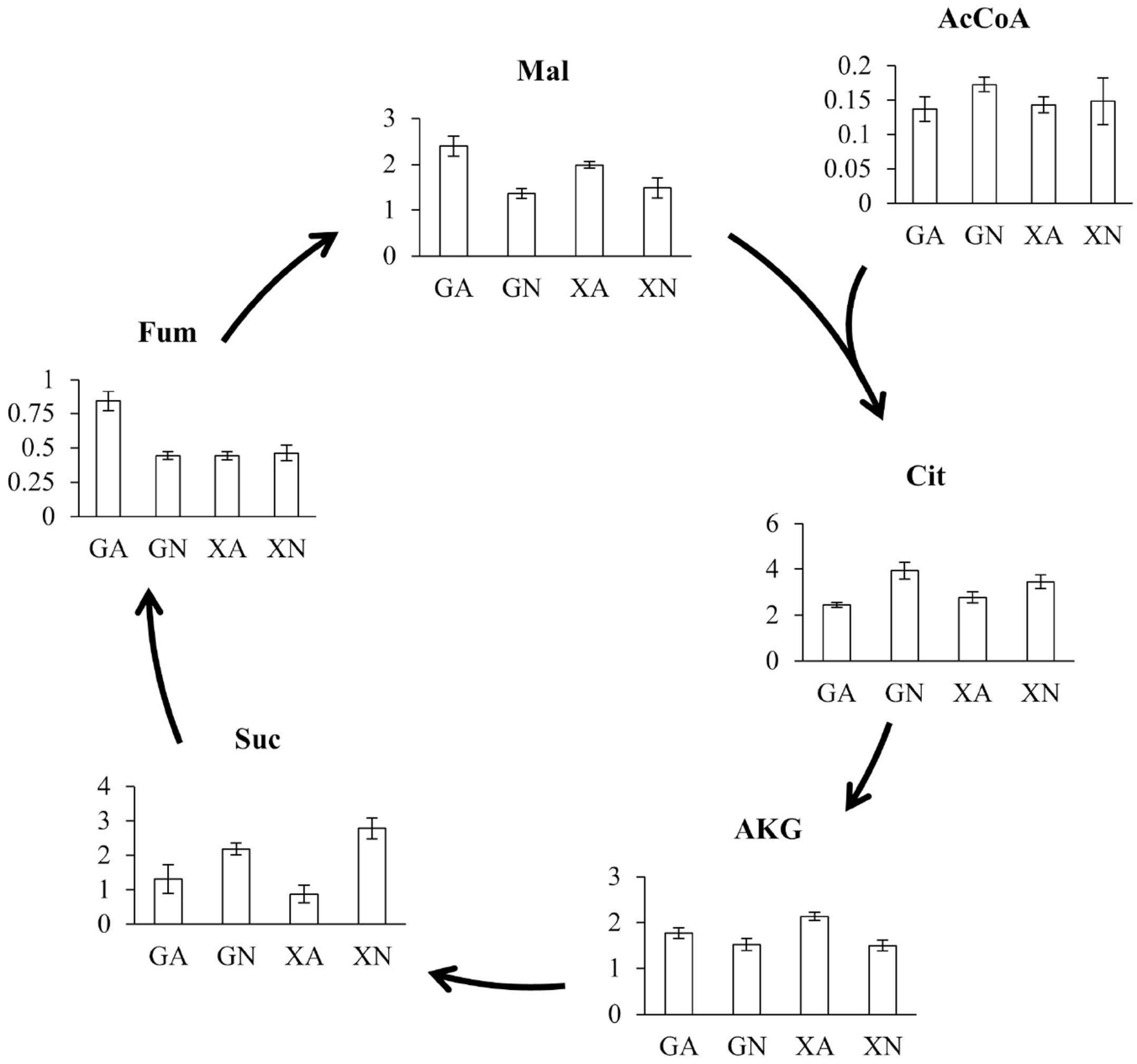

Fig. 2.

Metabolite pool sizes for metabolites in the TCA Cycle. All pool sizes are in units of μmol/g DCW. Error bars represent uncertainties from standard deviations of three biological replicates as well as uncertainties in OD_{600}-DCW correlations. GA = Glucose Aerobic, GN = Glucose Anaerobic, XA = Xylose Aerobic, XN = Xylose Anaerobic

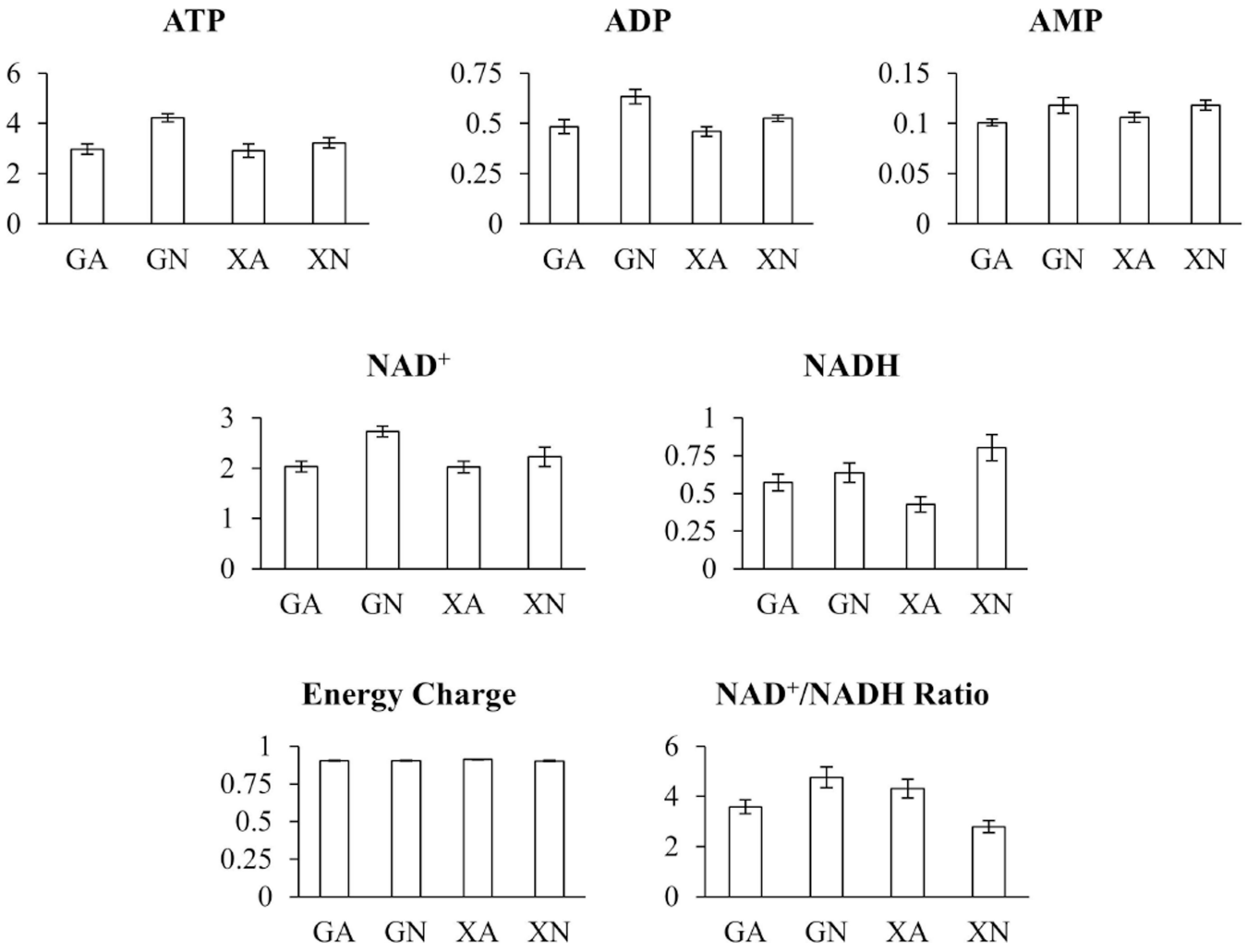

Fig. 3.

Metabolite pool sizes and ratios for select cofactors. All pool sizes are in units of μmol/g DCW. Pool size error bars represent uncertainties from standard deviations of three biological replicates as well as uncertainties in OD_{600}-DCW correlations. Metabolite ratio error bars represent uncertainties from standard deviations of three biological replicates only. GA = Glucose Aerobic, GN = Glucose Anaerobic, XA = Xylose Aerobic, XN = Xylose Anaerobic

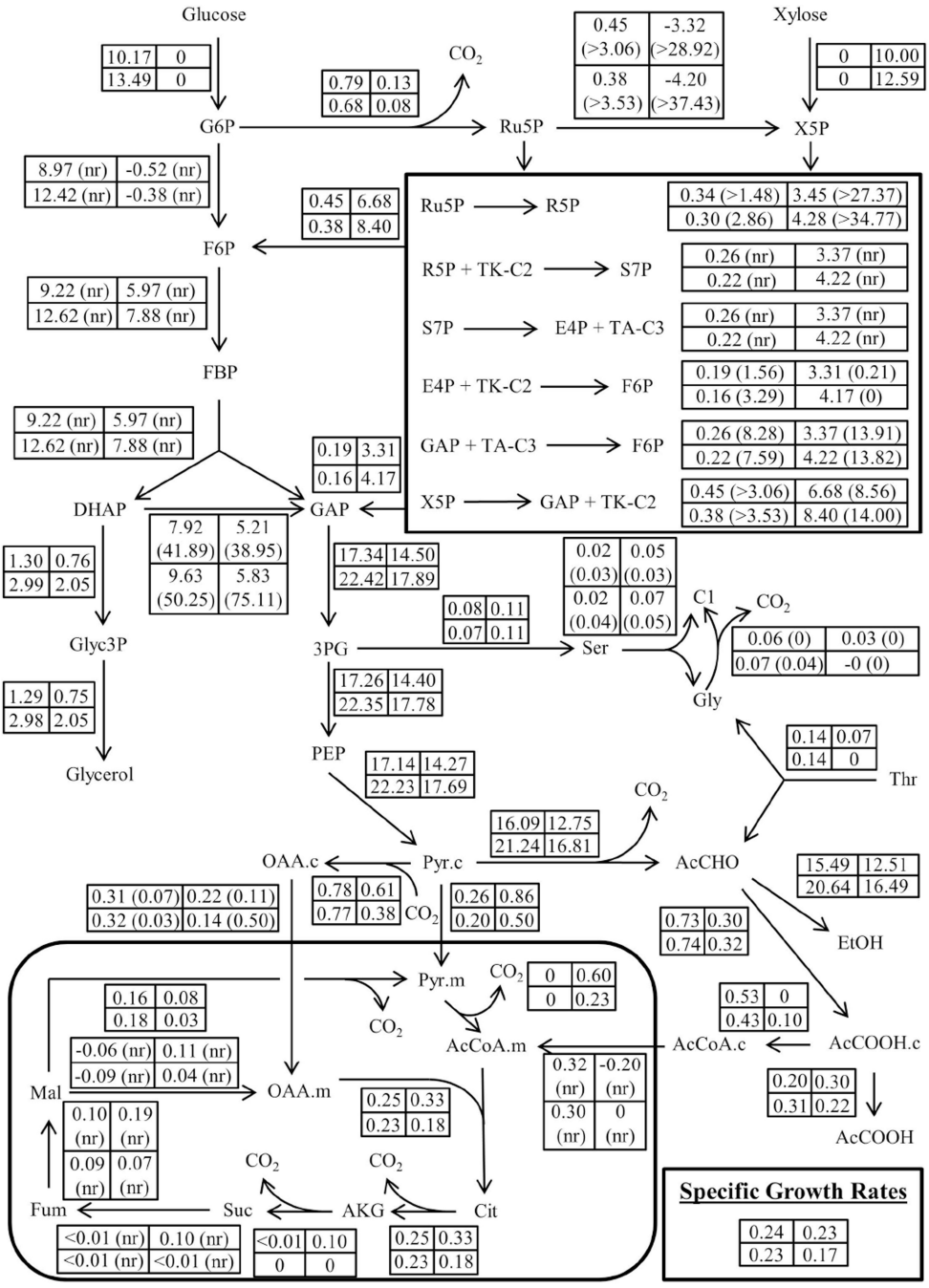

Fig. 4.

Best-fit metabolic flux distributions in xylose-consuming *S. cerevisiae* strain under four sets of conditions. All fluxes are given in units of mmol/g/h. For each reversible reaction the net flux is given with the exchange flux indicated inside parentheses; “nr” indicates the exchange flux could not be resolved to within one order of magnitude. Specific growth rates (shown in the bottom right of the Figure) are in units of h^{-1}. Four values are listed for each flux. These are the best-fit values for the Glucose Aerobic (top left), Glucose Anaerobic (bottom left), Xylose Aerobic (top right), and Xylose Anaerobic (bottom right) cultures

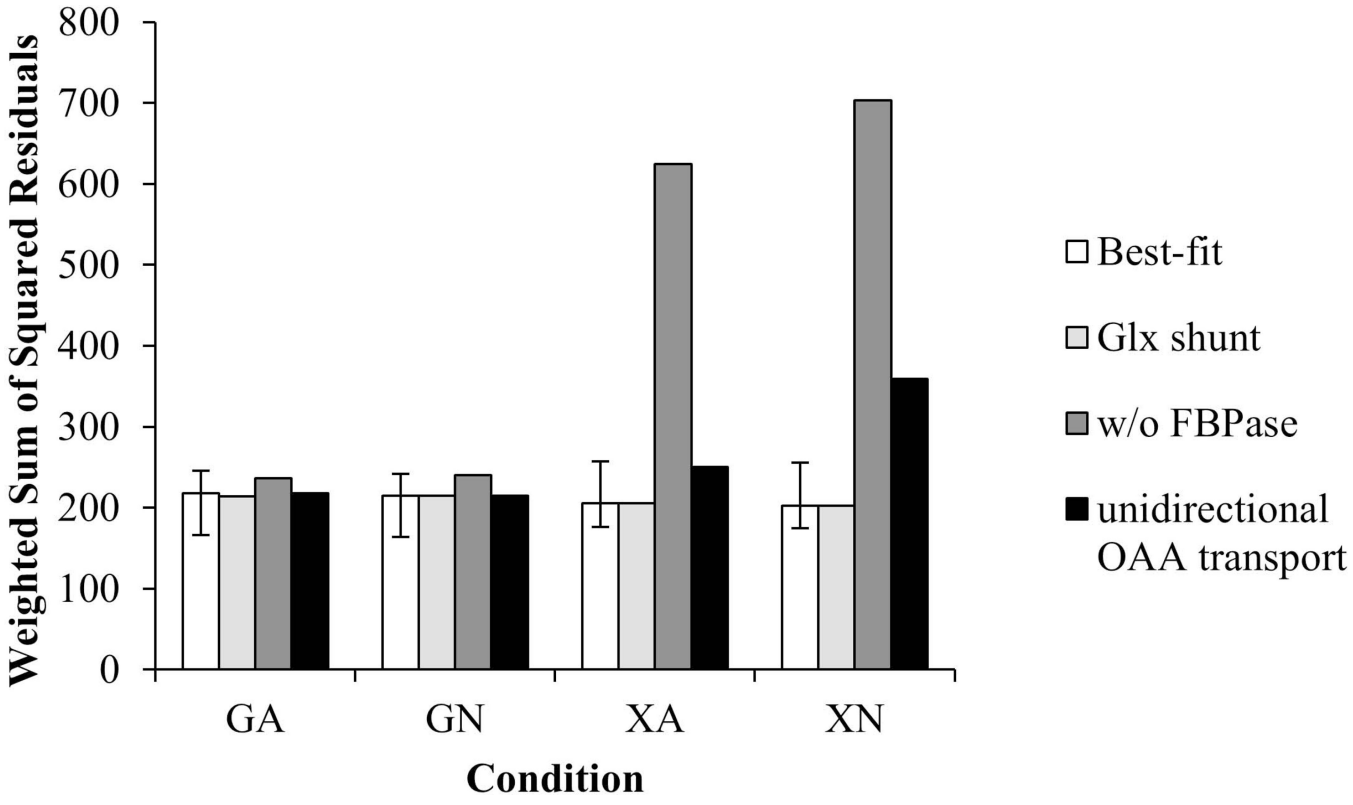

Fig. 5.

Weighted Sums of Squared Residuals from flux estimations with different models. “Best-fit” = the final metabolic model used for flux estimation, “Glx shunt” = the final model with addition of the glyoxylate shunt pathway, “w/o FBPase” = the final model with removal of the gluconeogenic enzyme Fructose-1,6-Bisphosphatase, “unidirectional OAA transport” = the final model with removal of OAA transport from mitochondria to cytosol (i.e. via Malate-Aspartate or Malate-Oxaloacetate Shuttle), so that OAA can only be transported from cytosol to mitochondria. Error bars for each “Best-fit” model show the expected range for the weighted sum of squared residuals in the chi-square goodness-of-fit test. GA = Glucose Aerobic, GN = Glucose Anaerobic, XA = Xylose Aerobic, XN = Xylose Anaerobic

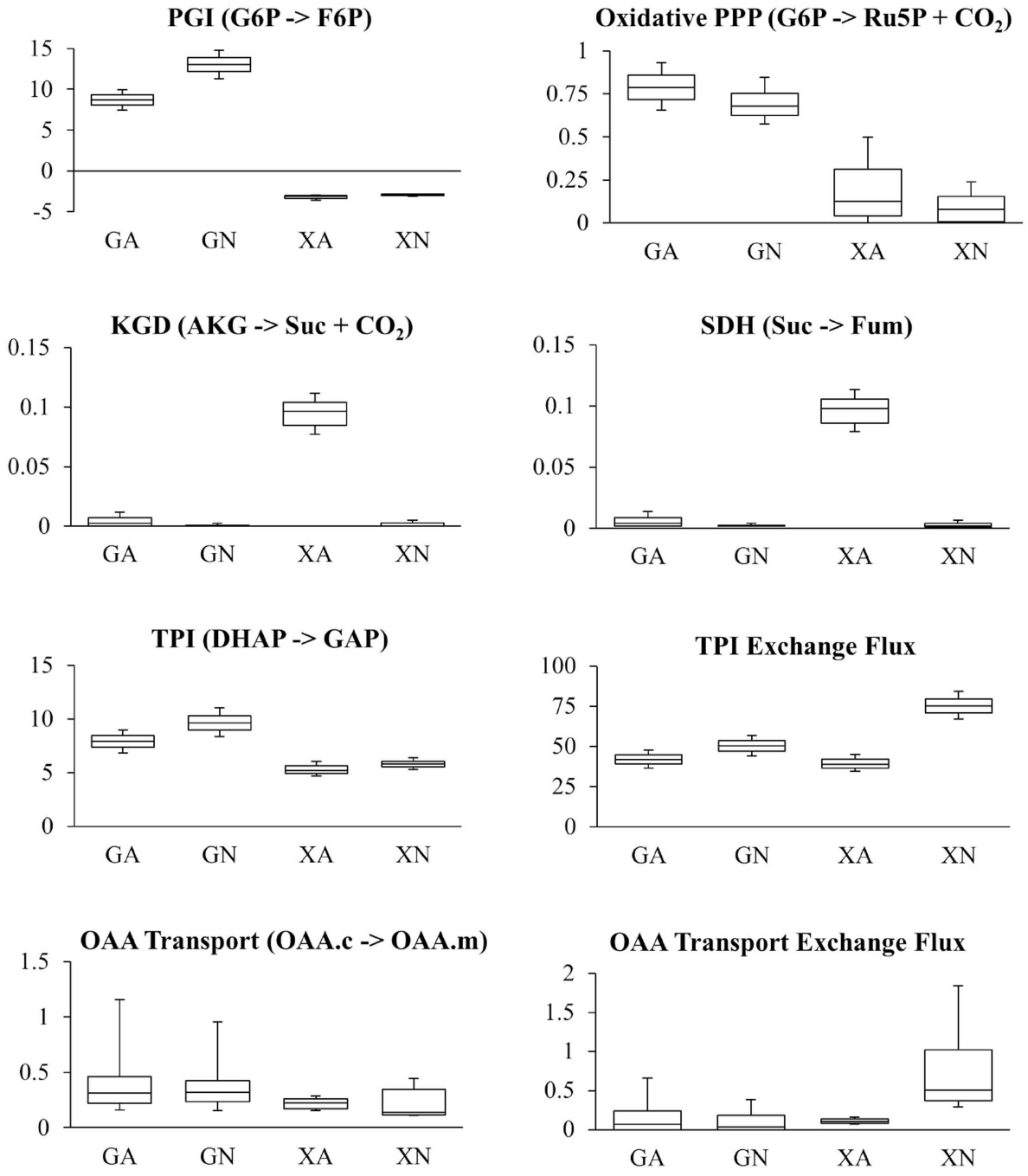

Fig. 6.

Confidence intervals for select fluxes. All fluxes are in units of mmol/g/h. The line inside each box represents the best-fit value of the flux. Each box represents the flux 68% confidence interval and the error bars ("whiskers") represent the flux 95% confidence interval. GA = Glucose Aerobic, GN = Glucose Anaerobic, XA = Xylose Aerobic, XN = Xylose Anaerobic. Enzyme abbreviations: PGI, Phosphoglucose isomerase; KGD, α-

Ketoglutarate dehydrogenase; SDH, Succinate dehydrogenase; TPI, Triosephosphate isomerase

Table I

Specific growth rates and specific metabolite consumption and production rates under different growth conditions. GA = Glucose Aerobic, GN = Glucose Anaerobic, XA = Xylose Aerobic, XN = Xylose Anaerobic

Rate	GA	GN	XA	XN
μ (h^{-1})	0.243 ± 0.007	0.228 ± 0.003	0.231 ± 0.010	0.178 ± 0.006
$q_{glucose/xylose}$ (mmol/g/h)	−11.6 ± 1.9	−13.8 ± 1.3	−10.0 ± 1.4	−12.3 ± 3.1
$q_{ethanol}$ (mmol/g/h)	16.0 ± 1.1	20.6 ± 2.0	12.6 ± 1.3	14.8 ± 1.1
$q_{glycerol}$ (mmol/g/h)	1.28 ± 0.08	3.04 ± 0.32	0.75 ± 0.16	2.15 ± 0.18
$q_{acetate}$ (mmol/g/h)	0.21 ± 0.05	0.33 ± 0.05	0.32 ± 0.07	0.23 ± 0.05